Supporting Information

Stable, Ultralow Threshold Amplified Spontaneous Emission from $CsPbBr_3$ Nanoparticles Exhibiting Trion Gain

Yi Wang,[†] Min Zhi,[†] Yu-Qiang Chang[‡] Jian-Ping Zhang[‡] and Yinthai Chan[,†]*

[†]Department of Chemistry, National University of Singapore, 3 Science Drive 3, Singapore 117543, Singapore

[‡]Department of Chemistry, Renmin University of China, 59 Zhongguancun Street, Beijing 100872, China

Corresponding Author

*E-mail: chmchany@nus.edu.sg

1. *Determining the theoretical threshold for trion based gain*

Within the framework of a Poisson distribution, the probability of generating N excitons per colloidal quantum dot (CQD) is given as $p_N = (\langle N \rangle^N / N!) \exp(-\langle N \rangle)$, where $\langle N \rangle$ is the average number of excitons per CQD. For the competition between reabsorption and stimulated emission processes that determines net optical gain in charged nanoparticles, three specific cases (i.e. p_0, p_1 and p_i ($i \geq 2$)) are taken into account as illustrated in Figure S1.

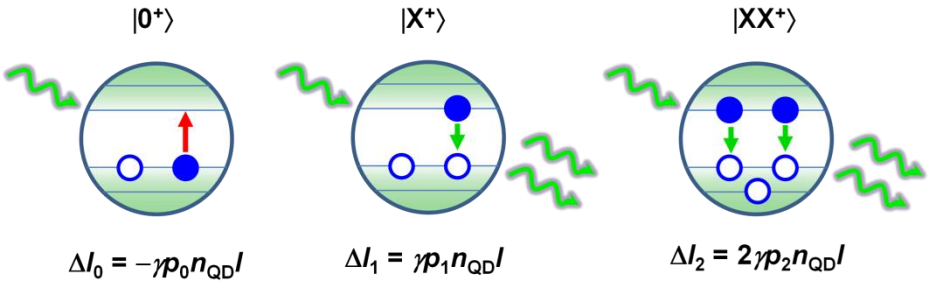

Figure S1. Schematic cartoon illustrating the absorption and stimulated emission of a charged nanoparticle in three cases: ground state ($|0^+\rangle$), singly excited state ($|X^+\rangle$) and doubly excited state ($|XX^+\rangle$). The two electrons/holes in the same energy level are distinguished by their spin directions.

If seed photons of intensity I are incident upon the various charged CQDs illustrated above, the resulting change in photon intensity may be estimated as follows:

$$\Delta I_0 = -\gamma p_0 n_{QD} I \quad \text{(S1)}$$

$$\Delta I_1 = \gamma p_1 n_{QD} I \quad \text{(S2)}$$

and

$$\Delta I_i = 2\gamma p_i n_{QD} I \quad \text{(where } i \geq 2\text{)} \quad \text{(S3)}$$

where γ is probability of electron-hole recombination (a negative value is taken to mean electron-hole formation), n_{QD} is the number density of charged QDs and the subscripts of ΔI and p refer to the exciton occupancy of a nanoparticle. Where $\sum \Delta I_i$ is positive, net optical gain is achieved. Combining

equation S1, equation S2 with equation S3, the boundary condition of optical gain is hence obtained as:

$$\sum_{i=0}^{\infty} \Delta I_i = \gamma n_{\mathrm{QD}} I \left(-p_0 + p_1 + 2\sum_{i=2}^{\infty} p_i \right) = 0 \quad \text{(S4)}$$

Inserting the expression of Poisson distribution into equation S4, one can get the theoretical threshold of trion gain as $\langle N \rangle_{\mathrm{th}} = 0.58$, and the probabilities of obtaining different exciton numbers per particle in this case are $p_0 = 0.56$, $p_1 = 0.32$ and p_{i} ($i \geq 2$) = 0.12 respectively.

2. *Determination of ⟨N⟩ at different pump fluence*

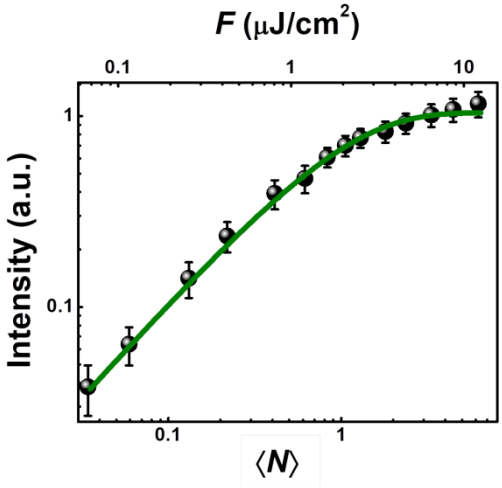

Figure S2. The PL intensity as a function of ⟨*N*⟩ or *F* in $CsPbBr_3$ CQDs. The circles are experimental data obtained from three independent measurements clearly exhibiting the saturation behaviour. The curve is the fitting results within the framework of Poisson distribution.

Based on the expression of Poisson distribution as discussed in above section, the single exciton PL intensity (I_{PL}) can be expressed as $I_{PL} \propto (1 - p_0) = 1 - \exp(-\sigma F)$, where σ is the cross-section, *F* is the pump fluence and $\langle N \rangle \equiv \sigma F$. By fitting the I_{PL}-*F* plot with this equation, one can obtain the value of σ for $CsPbBr_3$ CQDs, as illustrated in Figures S2, which then allows the value of ⟨*N*⟩ to be determined once *F* is known.

3. TRPL kinetics in $CsPbBr_3$ CQDs at ultra-low pump fluence

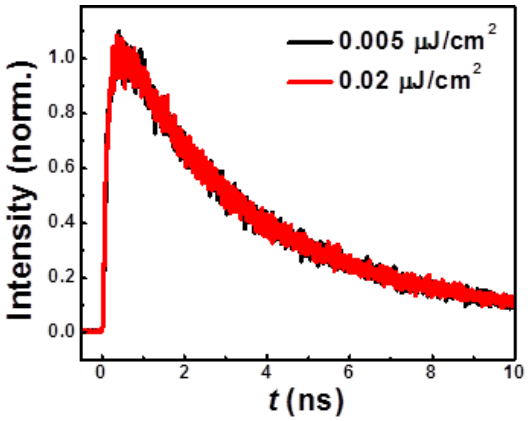

Figure S3. The TRPL decays of as-synthesized $CsPbBr_3$ CQDs in toluene under pump fluences of 0.005 μJ/cm^2 (black) and 0.02 μJ/cm^2 (red).

As evident in the figure above, there are no discernible differences between the PL decay kinetics recorded at pump fluences of 0.005 μJ/cm^2 and 0.02 μJ/cm^2. This implies that in both cases, the kinetics are dominated by single exciton recombination processes.

4. *Performing subtraction procedures to obtain τ_{X^*} and τ_{XX} of $CsPbBr_3$ CQDs*

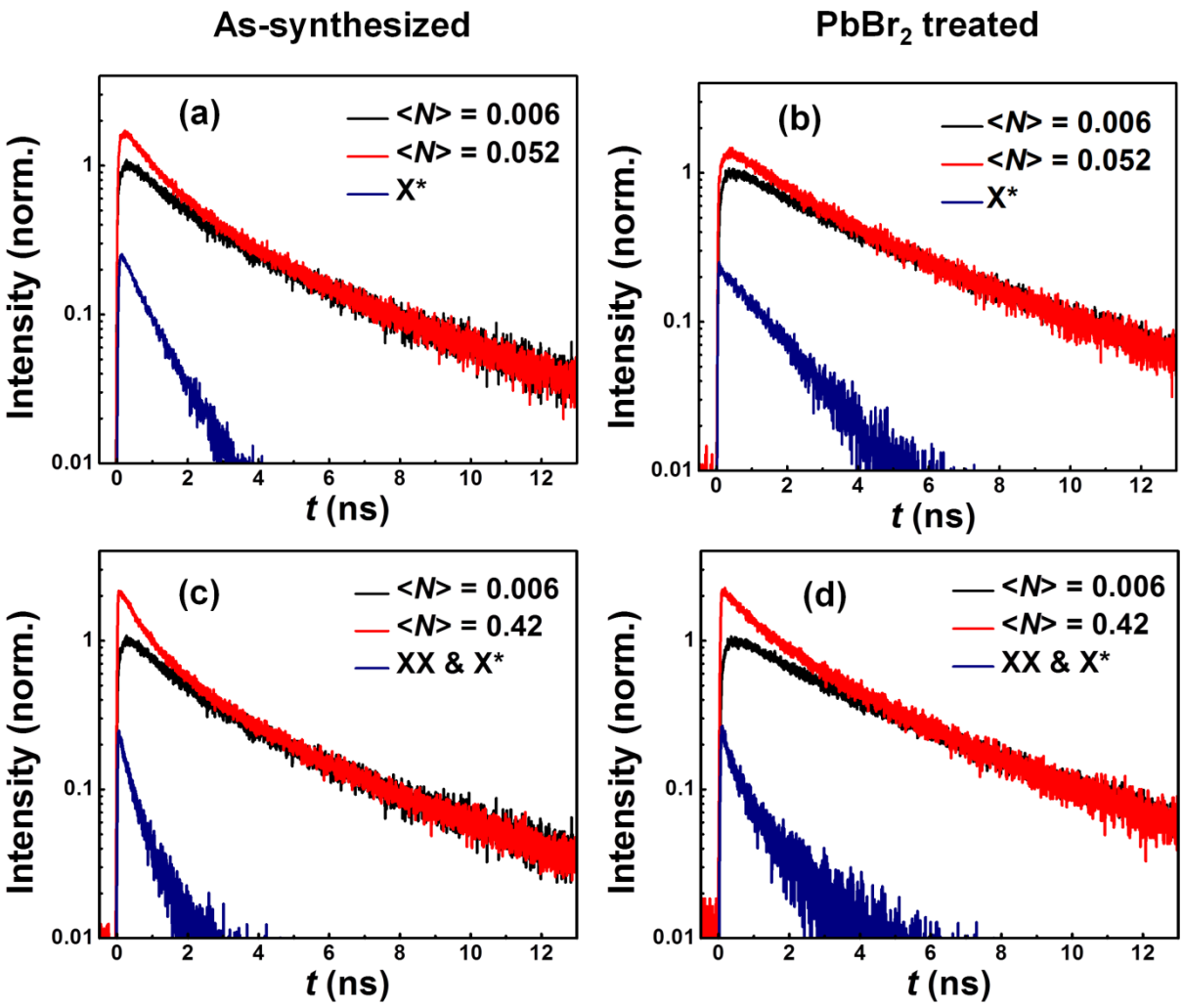

Figure S4. The TRPL kinetics of $CsPbBr_3$ CQDs at different pump fluences (black and red) which have been normalized at t = 8 ns and the subtracted results (blue). (a) and (c) correspond to the as-synthesized $CsPbBr_3$ CQDs, (c) and (d) correspond to the $PbBr_2$ treated $CsPbBr_3$ CQDs.

To analyze the dynamics of trion recombination, we performed subtraction procedures on the TRPL profiles recorded at excitation intensities corresponding to $\langle N \rangle < 0.1$, where the proportion of biexcitons and multi-excitons is statistically negligible. The results are shown in Figure S4a and Figure S4b, where it is seen that the removal of the single exciton contribution results in a mono-exponential decay that is ascribed to trion (X*) recombination. Fitting results give τ_{X^*} = 0.92 ns and 1.63 ns for the pristine and $PbBr_2$ treated $CsPbBr_3$ CQDs respectively (Figure 4c in main text).

Similarly, the same subtraction procedures are also performed on the TRPL kinetics recorded at excitation intensities corresponding to $\langle N \rangle = 0.42$ to gain insights into the recombination dynamics of biexcitons, as depicted in Figure S4c and Figure S4d. The resulting plots show biexponential decay profiles in which the faster (τ_1) and slower (τ_2) components are assigned to biexciton and trion recombination respectively. The fitting parameters are summarized in Table S1, where it is seen that the values of τ_2 and τ_{X^*} are in close agreement with each other. Note that the probability of multi-exciton formation (i.e. $N > 2$) is less than 0.2% at $\langle N \rangle = 0.42$, which explains why the recombination of multiexcitons is not detected in this measurement.

Table S1. The parameters for fitting the TRPL decays obtained from the subtraction procedure in Figure S4c and S4d with biexponential functions. A_i and τ_i (i = 1 or 2) are the pre-exponential factor and decay lifetime of the ith exponential component respectively. τ_{X^*} is the lifetime of the trion obtained from the measurements shown in Figure S4a and S4b.

Parameters	A_1	τ_1	A_2	τ_2	τ_{X^*}
Untreated	63.8%	0.31 ns	36.2%	1.00 ns	0.92 ns
$PbBr_2$ treated	59.6%	0.32 ns	40.4%	1.60 ns	1.63 ns

5. TRPL kinetics of multiexciton recombination

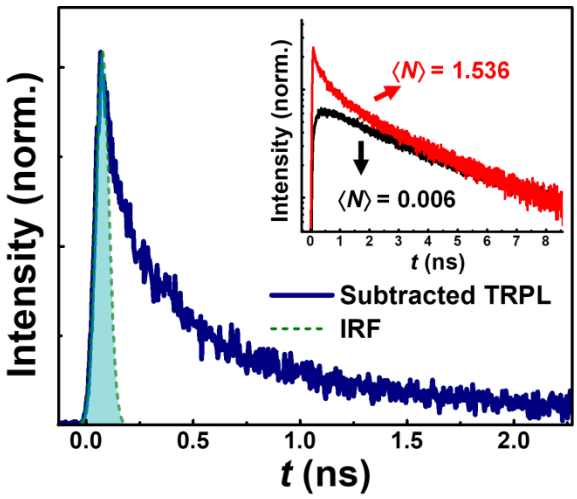

Figure S5. The TRPL kinetics of $CsPbBr_3$ CQDs obtained by subtracting the PL trace at $\langle N \rangle = 0.006$ (black curve in inset) from the one at $\langle N \rangle = 1.536$ (red curve in inset). The purple curve is the result of the subtraction procedure and the dashed green line represents the IRF of the TCSPC setup.

Figure S5 shows the TRPL kinetics obtained by subtracting the kinetics trace at $\langle N \rangle = 0.006$ from the one at $\langle N \rangle = 1.536$, where an ultra-fast decay component within the IRF is seen and likely results from recombination processes involving multi-excitons. The probability of multi-exciton formation is estimated to be as high as 20% which lends support to this assertion.

6. *Characterization of the $CsPbBr_3$ films*

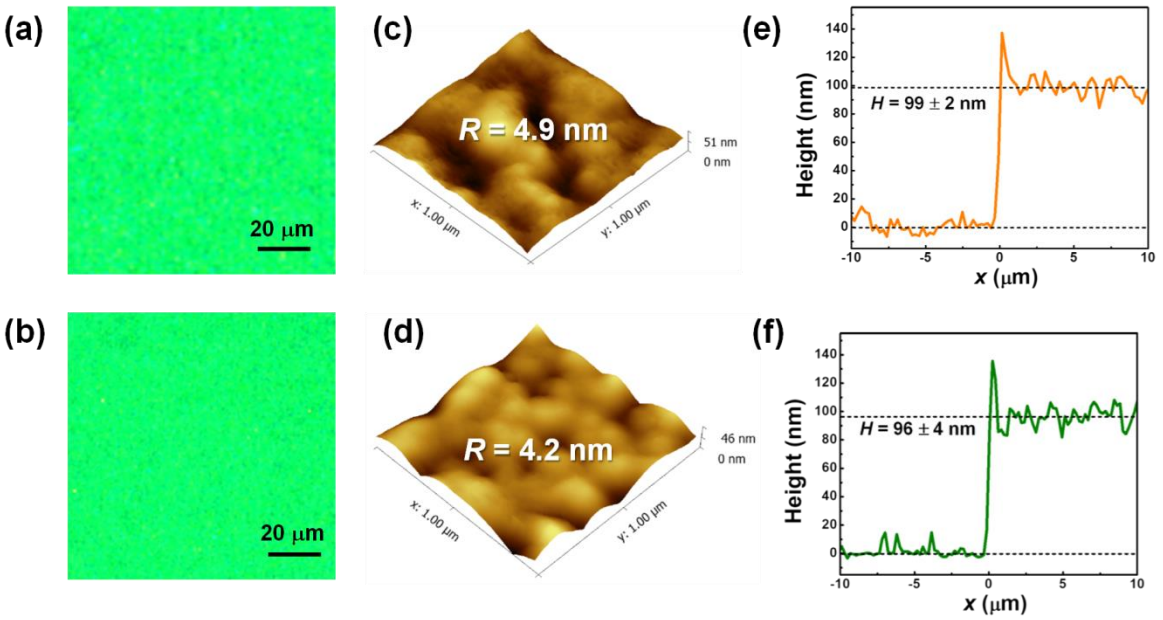

Figure S6. (a, b) Fluorescence microscope images, (c, d) AFM images and (e, f) cross-sectional thickness profiles of $CsPbBr_3$ films, where the upper and lower panels correspond to the untreated and $PbBr_2$ treated films respectively.

7. TRPL kinetics of $CsPbBr_3$ films below and above ASE threshold

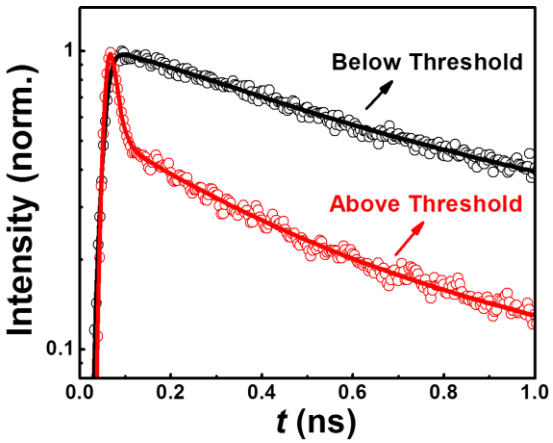

Figure S7. The TRPL traces in a $CsPbBr_3$ film pumped below (~0.8F_{th}, black) or above (~1.2F_{th}, red) the ASE threshold (denoted as F_{th}). The open circles are experimental data and the solid lines are fits to the curves.

It is readily seen in Figure S7 the emergence of an ultra-fast decay component whose kinetics are beyond the temporal resolution of our TRPL setup as the pump fluence exceeds the ASE threshold of the $CsPbBr_3$ film. Different from the fast decay shown in Figure S5, this ultra-fast kinetics cannot be attributed to multi-exciton recombination because the probability of multi-exciton formation (p_i, $i \geq 3$) is too small (< 0.04) to be detected with a pump fluence of 1.2F_{th}. Along with the data shown in Figure 5c and 5d in the main text, this ultra-fast decay provides strong evidence for the occurrence of ASE.

8. Comparison of ASE threshold of $CsPbBr_3$ film reported in different works

Table S2. A summary of the optically pumped ASE threshold values of $CsPbBr_3$ films in the literature and in this work.

References	Ref. S1	Ref. S2	Ref. S3	Ref. S4	In this work	
					As-synthesized	$PbBr_2$ treated
F_{th} ($\mu J/cm^2$)	2.1	2.2	5	22	3.8	1.2
Excitation Wavelength	400 nm	405 nm	400 nm	400 nm	400 nm	
Pulse Width	100 fs	50 fs	100 fs	100 fs	100 fs	
Stripe Length	–	0.6 cm	0.75 cm	0.75 cm	0.8 cm	

9. *Effect of $PbBr_2$ treatment on ASE thresholds of different $CsPbBr_3$ films*

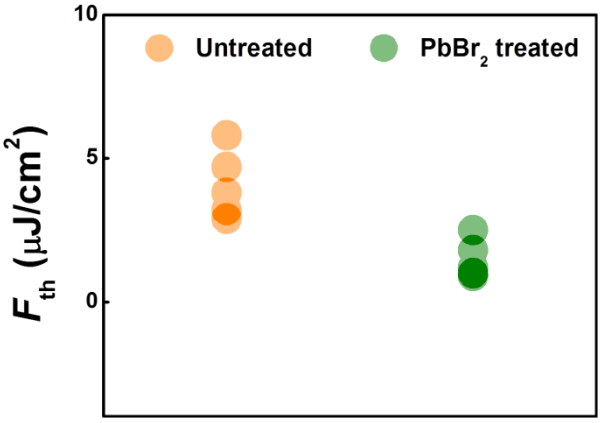

Figure S8. The histogram plot of ASE thresholds of 5 different sets of untreated (orange) and $PbBr_2$ treated (green) $CsPbBr_3$ film samples.

To ascertain that the $PbBr_2$ treatment improves the ASE thresholds of films of $CsPbBr_3$ CQDs in a robust manner, we prepared 5 different sets of $PbBr_2$ treated and untreated films over the course of 3 days under ambient conditions and determined their ASE thresholds. The nanoparticles in treated films only underwent the treatment process just before fabrication into a film. As readily seen in the Figure above, the ASE thresholds are significantly lower for $CsPbBr_3$ nanoparticles that had undergone $PbBr_2$ treatment.

References:

S1. Tong, Y.; Bladt, E.; Ayguler, M. F.; Manzi, A.; Milowska, K. Z.; Hintermayr, V. A.; Docampo, P.; Bals, S.; Urban, A. S.; Polavarapu, L.; Feldmann, J. *Angew. Chem. Int. Ed.* **2016,** *55*, 13887-13892.

S2. Imran, M.; Caligiuri, V.; Wang, M.; Goldoni, L.; Prato, M.; Krahne, R.; De Trizio, L.; Manna, L. *J. Am. Chem. Soc.* **2018,** *140*, 2656-2664.

S3. Yakunin, S.; Protesescu, L.; Krieg, F.; Bodnarchuk, M. I.; Nedelcu, G.; Humer, M.; De Luca, G.; Fiebig, M.; Heiss, W.; Kovalenko, M. V. *Nat. Commun.* **2015,** *6*, 8056.

S4. Wang, Y.; Li, X.; Song, J.; Xiao, L.; Zeng, H.; Sun, H.. *Adv. Mater.* **2015,** *27*, 7101-7108.